



Contents lists available at ScienceDirect

Journal of Alloys and Compounds

journal homepage: <http://www.elsevier.com/locate/jalcom>

Hard and adherent a-C:H gradient coatings by stress engineering

Liangliang Liu^a, Xiaokai An^a, Zhengyong Ma^a, Zhongzhen Wu^{a, b, *}, Wei Tang^a, Hai Lin^a, Ricky KY. Fu^b, Xiubo Tian^a, Paul K. Chu^b, Feng Pan^a^a School of Advanced Materials, Peking University Shenzhen Graduate School, Shenzhen 518055, China^b Department of Physics and Department of Materials Science and Engineering, City University of Hong Kong, Tat Chee Avenue, Kowloon, China

ARTICLE INFO

Article history:

Received 27 April 2018

Received in revised form

22 June 2018

Accepted 25 June 2018

Available online 27 June 2018

Keywords:

a-C:H

Stress engineering

High hardness

Adhesion

ABSTRACT

Hydrogenated diamond like carbon (a-C:H) coatings typically have low friction but high residual stress. The hardness which depends on the sp³ proportion increases not only the coating lifetime, but also the residual stress which can lead to easy film delamination especially for thick coatings. In this work, several thick a-C:H coatings (>10 μm) with different stress and hardness are prepared using stress engineering to mitigate stress accumulation while the hardness is retained. A low compressive residual stress of 0.42–0.84 GPa is achieved from the 8 μm thick a-C:H coating in addition to a high critical load of 63–74 N and hardness of over 26 GPa. The other desirable tribological and anticorrosion properties include a small friction coefficient of 0.13, low wear rate of 1.01 × 10⁻¹⁵ m³/N·m, high corrosion potential of -479.6 mV, as well as small corrosion current density of 1.77 μA/cm².

© 2018 Elsevier B.V. All rights reserved.

1. Introduction

Diamond like carbon (DLC) has attracted much commercial interest because of the tribological properties [1e3]. However, the hardness which depends on the sp³ proportion increases not only the coating lifetime, but also the residual stress which may lead to easy and premature delamination, particularly thick DLC coatings. Although DLC coatings with high hardness, excellent adhesion, or low residual stress have been reported [4–6], simultaneous demonstration of high hardness and low residual stress is still challenging [7–9].

Doping with Ti, Al, Ag, and Cu has been demonstrated to relax the structure to reduce the residual stress [10–13] and multilayered structures with metal interlayers have also been suggested [14,15]. However, some of the properties are often compromised, for example, hardness reduced to less than 20 GPa. Despite recent advance, fabrication of thick DLC films (>10 μm) with high hardness and good adhesion is still difficult [16–20]. In our previous studies [21,22], pulsed kV biases were implemented to fabricate 10 μm thick a-C:H (hydrogenated DLC) coatings with adhesion improved to 73 N. It was observed that the bias which provided alternative implantation and deposition during DLC depositing had a

significant effect on the residual stress and hardness. With increasing pulsed bias, the residual stress was relieved but the hardness declined as well. Nonetheless, proper stress engineering offers the potential to prepare thick DLC coatings with both high hardness and low stress.

In this study, 12 μm thick DLC coatings with different stress between 0.3 and 2.6 GPa are fabricated using different biases. A stress engineering method is proposed based on the results to construct a gradient multilayer DLC coating, which have both high hardness and good adhesion. Our results show that the residual stress of the 8 μm thick DLC coatings is between 0.42 and 0.84 GPa and the maximum critical load of 74 N is obtained due to the small residual stress. At the same time, the hardness is over 26 GPa and excellent adhesion of 67 N is achieved.

2. Experimental details

A Si (100) wafer (10 mm × 50 mm) with a thickness 500 ± 10 μm and high-speed steel (HSS, Ø30 × 3 mm) were used as substrates. The HSS samples were polished with abrasive SiC papers to 1000 grits and then 1 μm diamond paste on a velvet cloth. The samples were ultrasonically cleaned sequentially in alcohol, acetone, and deionized water for 30 min each and then dried under flowing nitrogen before inserting into a multifunctional plasma surface modification and deposition system (100 cm in diameter and height of 80 cm). After the vacuum chamber was evacuated to a

* Corresponding author. School of Advanced Materials, Peking University Shenzhen Graduate School, Shenzhen 518055, China.
E-mail address: wuzz@pkusz.edu.cn (Z. Wu).

base pressure of 3×10^{-3} Pa, the substrate was cleaned with Ar ions at a pressure of 0.8 Pa and bias voltage of -600 V for 20 min. To enhance the adhesion strength with the substrate, an optimized Cr/CrCx/CrC interlayer [21] was produced with Ar (99.999% pure) and C_2H_2 (99.8% pure) using a Cr target by high-power impulse magnetron sputtering (HiPIMS) with pulses of 750 V, 50 Hz, 300 μ s. Finally, the DLC coating was deposited using an anode layer ion source at a power of 300 W at a pressure of 0.5 Pa (10 sccm Ar and 45 sccm C_2H_2) without sample rotation.

Stress engineering method is proposed to restrain the total residual stress of the coating and ensure the surface hardness by a multilayers coating structure (Fig. 1). The inner layers near the substrate have low residual stress while the top layers possess high hardness. Assuming that the stress accumulates linearly with coating thickness, the total residual stress of the whole coatings could be estimated by following equation 1 (Eq. (1)).

$$\sigma = \sum_{i=1}^n \sigma_i T_i \quad (1)$$

Where σ is the total residual stress and σ_i and T_i is the unit thickness's residual stress and thickness of the i -th layer, respectively.

The thickness and morphology were measured by field-emission scanning electron microscopy (FE-SEM, ZEISS SUPRA[®] 55) and the chemical structure was determined at room temperature by high-resolution confocal Raman scattering (Horiba LabRam HR VIS with a 532 nm laser) and X-ray photoelectron spectroscopy (ESCALAB 250X, Thermo Fisher, England, with a pass energy of 20 eV and analysis time of 50 ms). The microhardness was determined by nanoindentation (NHT², Anton Paar, Austria) at a maximum load of 25 mN and a scratch test instrument (WS-2005, Zhongke Kaihua Technology, China) was employed to determine the adhesion strength between the film and substrate. The load was progressively increased from 0 N to 100 N at 3 mm/min and 50 N/min. The residual stress was measured by a film stress tester (FST100, SuPro Instruments, China), which is calculated by Stoney equation based on substrate curvature method (SCM) (Eq. (2)).

$$\sigma_f = \frac{E_s t_s^2}{6(1 - \mu_s) t_f} \left(\frac{1}{R_1} - \frac{1}{R_0} \right) \quad (2)$$

Where E_s , μ_s are the Young's modulus and Poisson's ratio of the substrate, respectively. t_f , t_s are the thicknesses of thin film and substrate, respectively. R_0 and R_1 are the substrate curvature radius before and after the film deposition. The substrate curvature radius is obtained by Laser Beam Deflection Technique which is particular precise even with tiny substrate deformation. A ball-on disk tester (MFT-5000, Rtec Instruments, America) was utilized to determine the friction coefficients and wear resistance properties at a relative humidity of $65 \pm 1\%$ RH and temperature of 25 ± 1 °C. A $\phi 3$ mm Si_3N_4 ball was used against the coatings at 4 N and 200 rpm with a

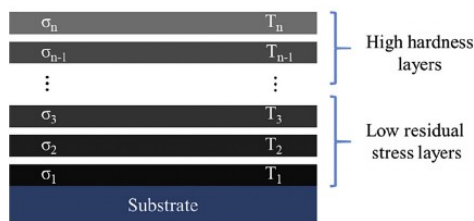


Fig. 1. The diagram of stress and hardness design.

wear radius of 5 mm. The corrosion resistance properties were determined on an electrochemical workstation (CHI-604E, Shanghai Chenhua).

3. Results and discussion

The hardness and residual stress of the a-C:H coatings fabricated under different biases are presented in Fig. 2. There is an obvious decline in the hardness and compressive residual stress with increasing biases. The largest hardness is 27 GPa and smallest stress is only -0.3 GPa but they are not observed from the same sample. Since the thickness of the coatings is 12 μ m, the average stress of each micron a-C:H coatings fabricated with pulsed DC bias of -800 V, -3500 V, -5500 V, -7500 V and -9500 V are 0.217 GPa, 0.100 GPa, 0.060 GPa, 0.033 GPa and 0.025 GPa, respectively. Based on these data and the corresponding deposition conditions, the residual stress is modified according to the method listed in Table 1 and a-C:H coatings with various architectures are fabricated by different step-decreasing biases. Consequently, the a-C:H coatings are expected to have low residual stress below 1.09 GPa (details shown in Table 1) while the highest hardness is retained on the coating surface.

The cross-sectional SEM images of the samples with different architectures are presented in Fig. 3. The coatings have similar thickness, about 8 μ m for the a-C:H coatings and 1.0 μ m for the Cr/CrCx/CrC interlayer which forms a continuous transition from the substrate to the a-C:H coatings without significant lattice mismatch as demonstrated by L.L. Liu et al. [21]. The a-C:H layers have a dense and amorphous structure without obvious grain boundaries, but some fuzzy interfaces are observed from the a-C:H layers because of the bias change during deposition. To differentiate the important top a-C:H layer (fabricated at -800 V) and the bottom a-C:H layer (fabricated at -9500 V), the interfaces are marked in Fig. 3. As shown in Table 1, the thickness of the bottom a-C:H layer with the smallest stress is between 4 μ m and 1 μ m and that of the top a-C:H layer with the highest hardness is between 1 μ m and 4 μ m depending on the deposition time. In between the top and bottom a-C:H layers, there are three a-C:H layers with a thickness of 1 μ m with gradually increasing hardness and stress.

Fig. 4(a) depicts the Raman scattering spectra of the four samples with different architectures. The peaks can be deconvoluted into the D and G peaks using the Gaussian fitting as shown in Table 2. Few differences can be observed from the peak position, the FWHM (full-width at half-maxima), and intensity ratio of the D

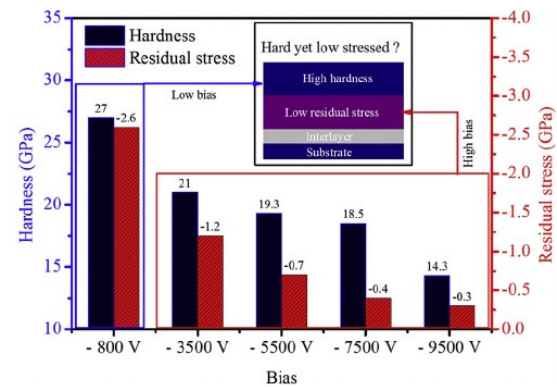


Fig. 2. Hardness and residual stress of the 12 μ m thick a-C:H coatings fabricated at different biases.

Table 1
Important instrumental parameters for fabrication of the a-C:H coatings.

Sample	Period I 9500 V	Period II 7500 V	Period III 5500 V	Period IV 3500 V	Period V 800 V	Expected Residual stress
1	4 μm	1 μm	1 μm	1 μm	1 μm	0.51 GPa
2	3 μm	1 μm	1 μm	1 μm	2 μm	0.70 GPa
3	2 μm	1 μm	1 μm	1 μm	3 μm	0.89 GPa
4	1 μm	1 μm	1 μm	1 μm	4 μm	1.09 GPa

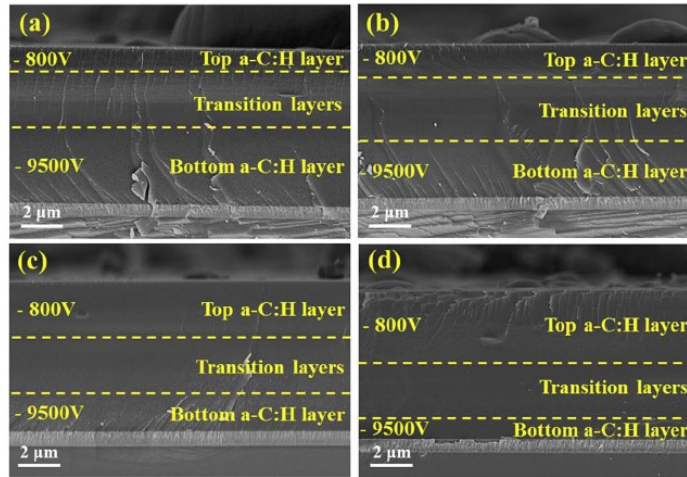


Fig. 3. SEM cross-sectional images: (a) Sample 1, (b) Sample 2, (c) Sample 3, (d) Sample 4.

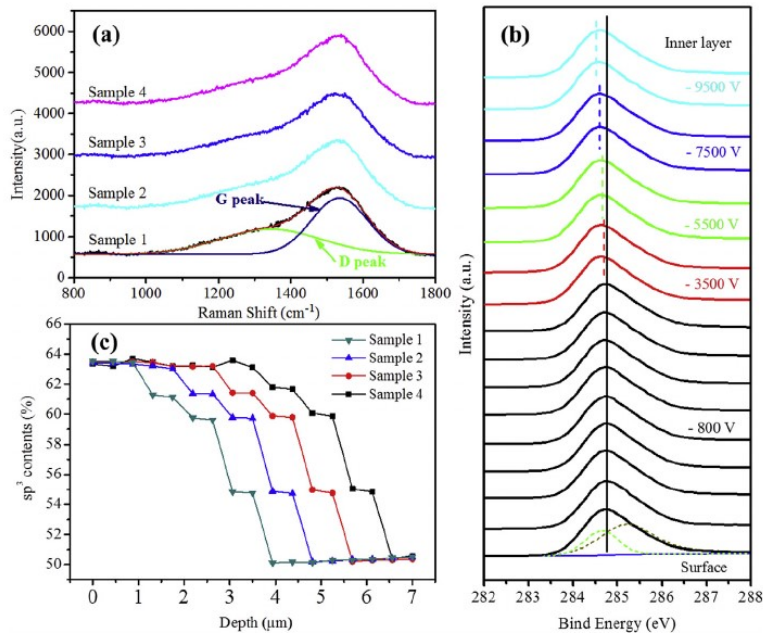


Fig. 4. Bonding structures: (a) Raman scattering spectra; (b) XPS of sample 4 at different depths; (c) sp^3 contents of different samples at different depths.

Table 2

Variations in the D and G peaks of the a-C:H coatings.

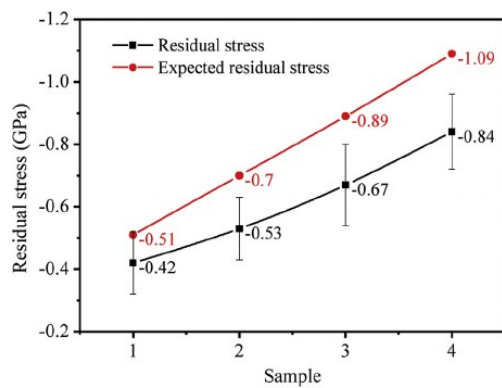
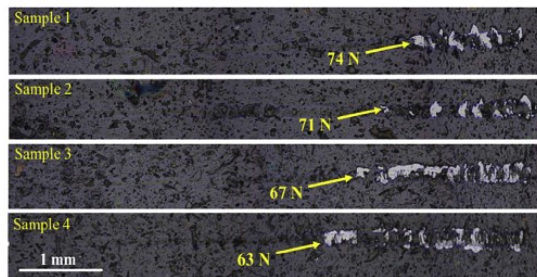
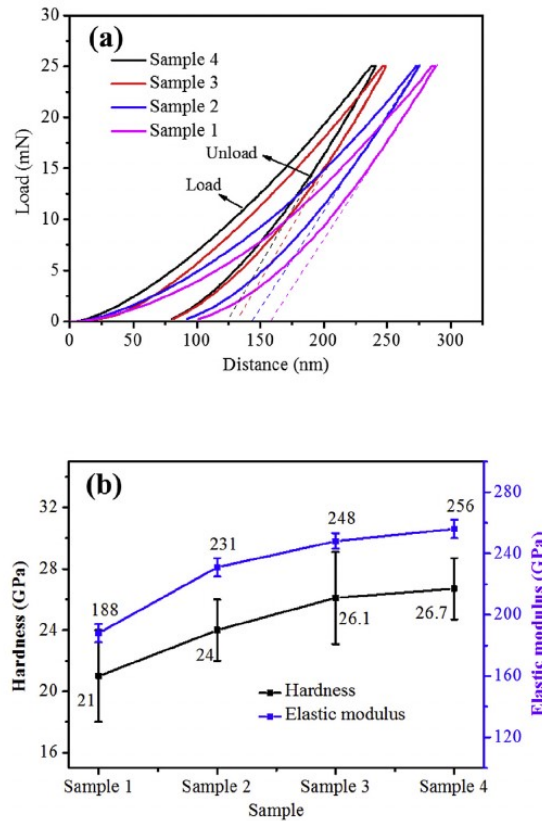
Sample	D band position (cm ⁻¹)	D FWHMD (cm ⁻¹)	G band position (cm ⁻¹)	G FWHMD (cm ⁻¹)	I _D /I _G
1	1343.64	277.92	1534.73	155.81	0.610
2	1343.61	277.89	1534.69	154.97	0.610
3	1343.20	281.13	1534.51	156.9	0.609
4	1344.23	281.91	1534.99	155.1	0.610

and G peaks, indicating that the sp^3 content in the top a-C:H layer is similar due to the same depositing parameters [23,24]. The depth profiles of the a-C:H coatings are obtained by monitoring the C1s peak during argon sputtering by XPS and the depth profile of sample 4 is shown in Fig. 4(b) as an example (those of other three samples are similar). The C1s spectra show large asymmetrical peaks and obvious shifts towards lower binding energy with depth indicating decreasing sp^3 content [25,26]. The spectra are deconvoluted into two peaks assigned to the C-C sp^2 hybridized carbon atoms (284.3 eV) and C-C sp^3 hybridized carbon atoms (285.2 eV). The calculated sp^3 contents at different depths in Fig. 3(c) decreases with depth corresponding to the applied bias during fabrication [22].

The residual stress is measured and compared with the expected stress calculated by simply superposition according to the stress engineering schemes (Fig. 5). The residual stress, which is compressive in all of the a-C:H coatings, increases slightly from 0.42 GPa to 0.84 GPa with increasing thickness of the top hard a-C:H layer. With enhancement by the pulsed bias, the decreased sp^3 fraction and effective dissipation of excess heat generated by the

ion impingement relax the compressive stress [16,27]. Therefore, a larger percentage of the top a-C:H layer brings larger stress in the whole DLC coatings attributed to the residual stress evolution between samples. It is noted that the measured residual stress is less than the expected one. This phenomenon is mainly attributed to the two assumes in the stress engineering: one is that the ignored stress difference occurred between the a-C:H samples with different bias and the Cr/CrCx/CrC interlayer and the other one is the different stress relaxation effect between the gradient a-C:H coatings and the single-phase a-C:H layer [28,29].

As reported previously, stress affects the adhesion strength between the coating and substrate. The adhesion strength of the a-C:H coatings is determined by scratch tests in which five scratches are made on each sample but no significant difference (± 1 N) is observed as shown in Fig. 6. The critical load between the coating and substrate decreases from 74 N to 63 N when the stress of the

**Fig. 5.** Residual stress of different samples.**Fig. 6.** Scratch test results of the a-C:H coatings.**Fig. 7.** Nanoindentation results: (a) Load versus displacement curves and (b) Hardness and elastic moduli.

coating increases from (0.42 ± 0.03) GPa to (0.84 ± 0.03) GPa with increasing the thickness of the top a-C:H layer, which has the largest stress for deposition at -800 V.

The hardness and elastic modulus of the a-C:H coatings deposited under different step-decreasing biases are determined by nanoindentation and shown in Fig. 7. The maximum indentation load is 25 mN. As shown in Fig. 7(a), the maximum penetration depth decreases with increasing thickness of the top a-C:H layer fabricated at -800 V, suggesting gradually increasing coating hardness (H) and elastic modulus (E). The hardness and elastic modulus determined from the load/displacement curves are presented in Fig. 7(b). The largest hardness is 26.7 GPa which is similar to that of the DLC coating prepared at a bias of -800 V as shown in Fig. 2. The hardness of the other samples is smaller because of the thinner top hard layer and influence of the relatively soft bottom layers [30]. Generally, the indentation depth cannot exceed the total film thickness by 10% in order to exclude the substrate effects [31e33]. The thicknesses of the top a-C:H layer in the two softer samples are 1 μm and 2 μm and 10% of them are smaller than the penetration depths of about 290 nm and 275 nm thus inducing the unavoidable “substrate effect” from the soft bottom layer. Since the top a-C:H layers are about 3 μm and 4 μm thick in the other two samples, no obvious difference can be observed from the hardness and modulus.

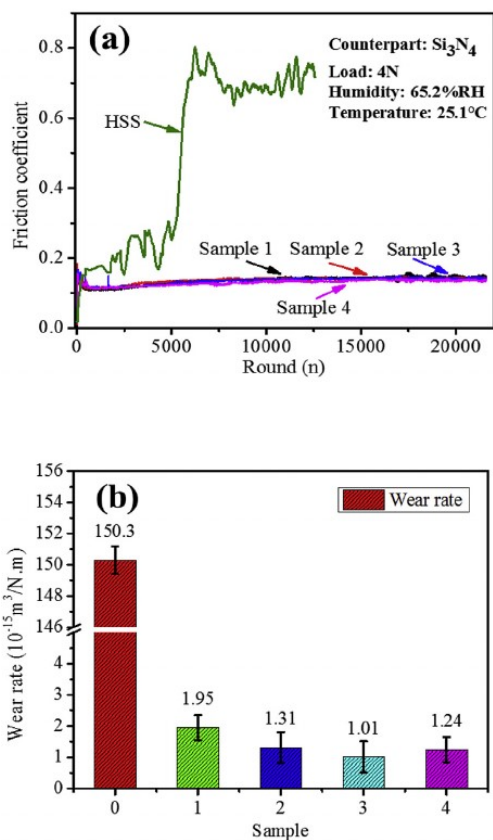


Fig. 8. Friction tests of HSS and a-C:H coatings: (a) Friction coefficients and (b) Wear rates.

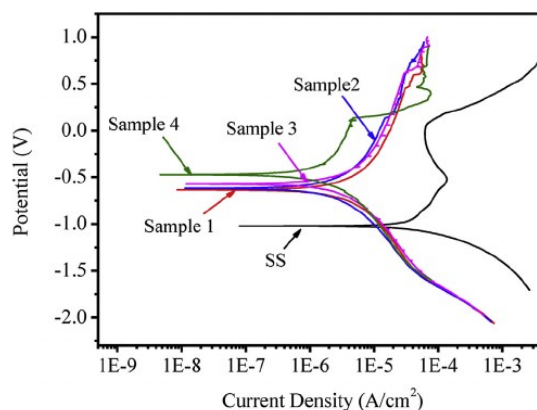


Fig. 9. Potentiodynamic tests of the SS substrate and different samples.

The friction coefficients and wear rates of the DLC coatings are determined by ball-on-disk tests with a Si₃N₄ counterpart for 2 h and the results are presented in Fig. 8 which also shows the friction coefficient of the HSS substrate for comparison. The fluctuation in the friction coefficients is much smaller than that of HSS and it stabilizes at about 0.13 until the end of the test indicating no destruction of the coatings. Fig. 8(b) shows the wear rates calculated by the wear volume. Compared to the poor wear resistance of HSS with a high wear rate of $(150.3 \pm 0.5) \times 10^{-15} \text{ m}^3/\text{N}\cdot\text{m}$, the four a-C:H samples exhibit much smaller wear rates of $(1.95 \pm 0.3) \times 10^{-15}$, $(1.31 \pm 0.4) \times 10^{-15}$, $(1.01 \pm 0.3) \times 10^{-15}$, and $(1.24 \pm 0.3) \times 10^{-15} \text{ m}^3/\text{N}\cdot\text{m}$, respectively, and the difference among the samples is minimal. The significantly enhanced wear resistance can be ascribed the large surface hardness and increased adhesion as a result of stress engineering.

The electrochemical corrosion behavior of the a-C:H samples and stainless steel (SS) substrate are investigated by potentiodynamic tests. The polarization curves and details about the corrosion current density (I_{corr}) and corrosion potential (E_{corr}) are shown in Fig. 9 and Table 3. Compared to the corrosion behavior of the SS substrate, all the a-C:H coatings show smaller I_{corr} and larger E_{corr} , indicating significantly improved corrosion resistance. As for the different architectures of the a-C:H coatings, higher E_{corr} and lower I_{corr} are obtained for thicker hard a-C:H layers. Owing to the large sp³ content which is closely related to the corrosion resistance [34], the hardest sample has the largest E_{corr} of -479.6 mV and smallest I_{corr} of $1.77 \mu\text{A}/\text{cm}^2$.

4. Conclusion

In order to fabricate a-C:H coatings with both high adhesion and hardness, a stress engineering scheme is designed. The residual stress of the 8 μm thick a-C:H coating is reduced to 0.42–0.84 GPa while high adhesion of to 63–74 N is observed. The surface

Table 3
 I_{corr} and E_{corr} of SS and different samples.

Sample	E_{corr} (mV)	I_{corr} ($\mu\text{A}/\text{cm}^2$)
SS	−1025	45.9
1	−639.2	7.78
2	−619.8	4.23
3	−572.4	3.76
4	−479.6	1.77

hardness exceeds 26 GPa, the friction coefficient is 0.13, and the wear rate is $1.01 \times 10^{-15} \text{ m}^3/\text{N}\cdot\text{m}$. In addition, excellent corrosion resistance as manifested by a large E_{corr} of -479.6 mV and small I_{corr} of $1.77 \mu\text{A}/\text{cm}^2$ is achieved. The stress engineering strategy can be extended to the other types of hard coatings to extend the service lifetime of engineering components.

Acknowledgements

This work was financially supported by Guangdong Science and Technology Research Grants (No. 2015B090927003), Shenzhen Science and Technology Research Grants (JCYJ20150828093127698 and GJHS20170313150213648), City University of Hong Kong Strategic Research Grant (SRG) No. 7004644, City University of Hong Kong Applied Research Grant (ARG) No. 9667122, as well as Hong Kong Research Grants Council (RGC) General Research Funds (GRF) No. CityU 11301215 and 11205617.

References

- [1] J. Robertson, Diamond-like amorphous carbon, *Mater. Sci. Eng. R Rep.* 37 (4–6) (2002) 129–281.
- [2] H.S. Zhang, J.L. Endrino, A. Anders, Comparative surface and nano-tribological characteristics of nanocomposite diamond-like carbon thin films doped by silver, *Appl. Surf. Sci.* 255 (5) (2008) 2551–2556.
- [3] M. Pandey, D. Bhattacharyya, D.S. Patil, et al., Structural and optical properties of diamond like carbon films, *J. Alloy. Comp.* 386 (1–2) (2005) 296–302.
- [4] A. Grill, Diamond-like carbon: state of the art. *Diam. Relat. Mater.* 8:428–434, *Diam. Relat. Mater.* 8 (2–5) (1999) 428–434.
- [5] J. Robertson, Diamond-like amorphous carbon, *Mater. Sci. Eng. R Rep.* 37 (4–6) (2002) 129–281.
- [6] K. Chiba, M. Tada, Buffered internal stresses in diamond-like carbon films reinforced with single-walled carbon nanotubes, *Thin Solid Films* 520 (6) (2012) 1993–1996.
- [7] A. Aijaz, T. Kubart, Ion induced stress relaxation in dense sputter-deposited DLC thin films, *Appl. Phys. Lett.* 111 (5) (2017), 051902.
- [8] Y. Wang, Y. Ye, H. Li, et al., A magnetron sputtering technique to prepare a-C:H films: effect of substrate bias, *Appl. Surf. Sci.* 257 (6) (2011) 1990–1995.
- [9] G. Capote, J.J. Olaya, V.J. Trava-Airoldi, Adherent amorphous hydrogenated carbon coatings on steel surfaces deposited by enhanced asymmetrical bipolar pulsed-DC PECVD method and hexane as precursor, *Surf. Coating. Technol.* 251 (29) (2014) 276–282.
- [10] X. Li, L. Sun, P. Guo, et al., Structure and residual stress evolution of Ti/Al, Cr/Al or W/Al co-doped amorphous carbon nanocomposite films: insights from ab initio calculations, *Mater. Des.* 89 (2016) 1123–1129.
- [11] J.H. Choi, S.C. Lee, K.R. Lee, A first-principles study on the bond characteristics in carbon containing Mo, Ag, or Al impurity atoms, *Carbon* 46 (2) (2008) 185–188.
- [12] X. Wang, W. Wu, S. Li, et al., Properties of W incorporated diamond-like carbon films prepared by pulsed-laser deposition, *J. Alloy. Comp.* 479 (1) (2009) 741–745.
- [13] D. Wei, A. Wang, Deposition and properties of Al-containing diamond-like carbon films by a hybrid ion beam sources, *J. Alloy. Comp.* 509 (13) (2011) 4626–4631.
- [14] A.A. Voevodin, S.D. Walck, J.S. Zabinski, Architecture of multilayer nanocomposite coatings with super-hard diamond-like carbon layers for wear protection at high contact loads, *Wear* 203 (96) (1997) 516–527.
- [15] F. Li, S. Zhang, J. Kong, et al., Multilayer DLC coatings via alternating bias during magnetron sputtering, *Thin Solid Films* 519 (15) (2011) 4910–4916.
- [16] L.F. Bonetti, G. Capote, L.V. Santos, et al., Adhesion studies of diamond-like carbon films deposited on Ti6Al4V substrate with a silicon interlayer, *Thin Solid Films* 515 (1) (2006) 375–379.
- [17] Ryeol Kim Wang, Min Seok Park, Uoo Chang Jung, et al., Effect of voltage on diamond-like carbon thin film using linear ion source, *Surf. Coating. Technol.* 243 (10) (2014) 15–19.
- [18] Y.J. Won, H. Ki, Effect of film gradient profile on adhesion strength, residual stress and effective hardness of functionally graded diamond-like carbon films, *Appl. Surf. Sci.* 311 (9) (2014) 775–779.
- [19] M. Lubwama, B. Corcoran, K. Sayers, et al., Adhesion and composite micro-hardness of DLC and Si-DLC films deposited on nitrile rubber, *Surf. Coating. Technol.* 206 (23) (2012) 4881–4886.
- [20] M. Kalin, I. Velkavrh, J. Vizintin, et al., Review of boundary lubrication mechanisms of DLC coatings used in mechanical applications, *Meccanica* 43 (6) (2008) 623–637.
- [21] L. Liu, Z. Wu, X. An, et al., Excellent adhered thick diamond-like carbon coatings by optimizing hetero-interfaces with sequential highly energetic Cr and C ion treatment, *J. Alloy. Comp.* 735 (2018) 155–162.
- [22] X.K. An, Z.Z. Wu, L.L. Liu, et al., High-ion-energy and low-temperature deposition of diamond-like carbon (DLC) coatings with pulsed kV bias, *Surf. Coating. Technol.* (2018) 173–177.
- [23] E. Enriquez, M.A.D.L. Rubia, A.D. Campo, et al., Characterization of carbon nanoparticles in thin-film nanocomposites by confocal Raman microscopy, *J. Phys. Chem. C* 1181 (19) (2014) 10488–10494.
- [24] A.C. Ferrari, J. Robertson, Resonant Raman spectroscopy of disordered, amorphous, and diamond like carbon, *Phys. Rev. B* 64 (7) (2001), 075414.
- [25] E. Ech-Chamikh, A. Essafi, Y. Jdijou, et al., XPS study of amorphous carbon nitride (a-C:N) thin films deposited by reactive RF sputtering, *Sol. Energy Mater. Sol. Cells* 90 (10) (2006) 1420–1423.
- [26] T. Ono, Y. Suda, M. Akazawa, et al., Effects of oxygen and substrate temperature on properties of amorphous carbon films fabricated by plasma-assisted pulsed laser deposition method, *Jpn. J. Appl. Phys.* 41 (7A) (2002) 4651–4654.
- [27] Y. Wang, Y. Ye, H. Li, et al., A magnetron sputtering technique to prepare a-C:H films: effect of substrate bias, *Appl. Surf. Sci.* 257 (6) (2011) 1990–1995.
- [28] X.C. Zhang, B.S. Xu, H.D. Wang, et al., Effects of compositional gradient and thickness of coating on the residual stresses within the graded coating, *Mater. Des.* 28 (4) (2007) 1192–1197.
- [29] V.V.S.S. Srikanth, T. Staedler, X. Jiang, Deposition of stress-free diamond films on Si by diamond/ β -SiC nanocomposite intermediate layers, *Diam. Relat. Mater.* 18 (10) (2009) 1326–1331.
- [30] M. Chhowalla, A.C. Ferrari, J. Robertson, et al., Evolution of sp² bonding with deposition temperature in tetrahedral amorphous carbon studied by Raman spectroscopy, *Appl. Phys. Lett.* 76 (11) (2000) 1419–1421.
- [31] Kumar S. Ishpal, N. Dwivedi, et al., Investigation of radio frequency plasma for the growth of diamond like carbon films, *Phys. Plasmas* 19 (3) (2012), 31–1.
- [32] D. Liu, G. Benstetter, E. Lodermeier, et al., Influence of the incident angle of energetic carbon ions on the properties of tetrahedral amorphous carbon (taC) films, *J. Vac. Sci. Technol. A Vac. Surf. Film* 21 (5) (2003) 1665–1670.
- [33] H. Liu, Q. Xu, C. Wang, et al., Investigating the microstructure and mechanical behaviors of DLC films on AISI52100 bearing steel surface fabricated by plasma immersion ion implantation and deposition, *Surf. Coating. Technol.* 228 (2013) S159–S163.
- [34] Z. Wang, C. Wang, Q. Wang, et al., Electrochemical corrosion behaviors of a-C:H and a-C:N_x:H films, *Appl. Surf. Sci.* 254 (10) (2008) 3021–3025.